Contrasting controls on $\delta^{18}O$-$\delta^{2}H$ and $\delta^{18}O$-$\delta^{17}O$ isotope systematics in a balance-filled lake

M.J. Custado, A.R. Waldeck, B. Belanger, X.-K. Wang, J.C.K. Rugenstein, K.M. Cobb, J.L. Oster, D.E. Ibarra

Supplementary Information

The Supplementary Information includes:

- Datasets and Code
- Physical and Hydroclimatic Setting of Bear Lake
- Isotope Notations
- Analytical and Data Reduction Methods
- Monte Carlo Implementation of the Lake Isotopic Mass Balance Equation
- Reconstruction of the $\delta^{18}O$ Composition of Unevaporated Catchment Precipitation ($\delta^{18}O_{rucp}$)
- Tables S-1 to S-6
- Figures S-1 to S-4
- Supplementary Information References

Datasets and Code

The isotopic dataset and Python scripts used for analysis and visualization can be found through the following link: https://doi.org/10.5281/zenodo.20819990. The master list spreadsheet file contains all data and geographic coordinates. The Python script used to reduce the Picarro L2140-i data output can be accessed through: https://doi.org/10.5281/zenodo.18356153.

Physical and Hydroclimatic Setting of Bear Lake

Situated within the northeastern Great Basin on the Utah-Idaho border, Bear Lake has been a critical water resource used for irrigation, flood management, and hydropower. Prior to around 1912, the lake was hydrologically disconnected from the Bear River, until an inlet canal was built to divert water to the lake which has since altered the lake's hydrology (Kaliser, 1972; Dean *et al.*, 2009). The lake is 32 km long with a maximum width of 12 km near the center. The lake's surface area is 282 km^2 at full capacity, with a maximum depth of 63 m and mean depth of 28 m (Birdsey, 1989; Dean

et al., 2009). The lake deepens from west to east, primarily due to the N-S trending fault on the eastern side of the lake (Dean *et al.*, 2009).

Chemical and hydrological changes in the lake since this diversion is detailed in Dean *et al.* (2007, 2009). Currently, Bear Lake is primarily an alkaline lake, with Ca^{2+}, Mg^{2+}, and HCO_3^- dominating the dissolved chemistry derived from the weathering of carbonate lithology in the Bear River Range (Fig. 1; Dean *et al.,* 2009). This region experiences hot, dry summer seasons and cold, wet winters, with evaporation still exceeding precipitation at annual basis, keeping the lake saturated with respect to carbonate minerals. Consequently, much of the water that enters the lake is in the form of snowmelt. This pronounced seasonality produces a distinct thermal and chemical stratification. During the late summer, specific conductance (25 °C) in the upper layers of the lake is approximately 685 µS cm^{-1}, increasing to approximately 700 µS cm^{-1} in the hypolimnion. The mean total dissolved solids (TDS) ranges from approximately 533 to 582 mg/L across the water column and similarly increase with depth (Dean *et al.*, 2007, 2009).

Isotope Notation

Raw isotope values (R) are the ratio of the rare isotope with the abundant isotope in the sample, normalized to the isotopic ratio of an internationally accepted standard. It is commonly reported using the delta (δ) notation and in per mil units (parts per thousand, ‰). The following equation is used to convert isotope ratios to δ values:

$$\delta = \left(\frac{R_{sample}}{R_{standard}} - 1\right) 1000 \qquad \text{Eq. S-1}$$

Analytical and Data Reduction Methods

The collected water samples were analysed for stable isotopes through cavity ring-down spectroscopy using a Picarro L2140-i unit. Three replicates of each sample were prepared in separate vials and were ran in different sequences. Following the protocols for memory and drift corrections from Hutchings and Konecky (2023), only the last three injections out of the six injections made for each vial were used in the data analysis. Additionally, we applied memory correction factors that were derived for the instrument from a separate analysis of internal standards. A linear regression of multiple replicates of an internal standard ("*Drift*") placed throughout the run sequence was used to correct for instrument drift. Internally calibrated ultrapure water was used as the drift correction standard.

Data were subsequently normalized using isotopically heavy and light internal standards (*"Heavy"* and *"Light,"* respectively) that bracket the isotopic range of the samples. These internal standards were calibrated against VSMOW2 and USGS reference materials (Table S-5). USGS46 standards were also analysed during each sequence to evaluate analytical accuracy (Table S-7).

The average of the last three injections per vial were taken as the $\delta^{17}O$, $\delta^{18}O$, and $\delta^{2}H$ data, while $\Delta'^{17}O$ was calculated for each injection using Eq. 4 before averaging. The final reported isotope values represent error-weighted averages of three measurement replicates (Eq. S-8).

Sample uncertainty calculations

Uncertainties for the $\delta^{17}O$, $\delta^{18}O$, and $\delta^{2}H$ data for each sample replicate were derived from the combined uncertainties of the calibrated internal standards and the standard deviations of the last three injections for each internal standard and sample following equation from Gröning (2011):

Eq. S-2

$$u(\delta_{sample}) = \left[\left(\frac{\partial f}{\partial \delta_{LS}}\right)^2 \cdot u(\delta_{LS})^2 + \left(\frac{\partial f}{\partial \delta_{HS}}\right)^2 \cdot u(\delta_{HS})^2 + \left(\frac{\partial f}{\partial \delta_{w\,LS}}\right)^2 \cdot u(\delta_{w\,LS})^2 + \left(\frac{\partial f}{\partial \delta_{w\,HS}}\right)^2 \cdot u(\delta_{w\,HS})^2 + \left(\frac{\partial f}{\partial \delta_{sample}}\right)^2 \cdot u(\delta_{sample})^2 \right]^{1/2}$$

where u is the reported (in the case for the internal standards) and measured uncertainties and δ is the reported or measured isotopic value. The subscripts correspond to either the sample, the calibrated value of the internal standards (*LS* for the light standard, and *HS* for the heavy standard). Terms with '*w*' as subscripts refer to the measured value of either HS or LS. The partial derivative terms are the variances of the different measurements and are calculated as:

$$\frac{\partial f}{\partial \delta_{LS}} = 1 - \frac{\delta_{sample} - \delta_{w\,LS}}{\delta_{w\,HS} - \delta_{w\,LS}} \quad \text{Eq. S-3}$$

$$\frac{\partial f}{\partial \delta_{HS}} = \frac{\delta_{sample} - \delta_{w\,LS}}{\delta_{w\,HS} - \delta_{w\,LS}} \quad \text{Eq. S-4}$$

$$\frac{\partial f}{\partial \delta_{w\,LS}} = \delta_{HS} - \delta_{LS} \cdot \frac{\delta_{sample} - \delta_{w\,LS}}{(\delta_{W\,HS} - \delta_{w\,LS})^2} - \frac{\delta_{HS} - \delta_{LS}}{\delta_{w\,HS} - \delta_{w\,LS}} \quad \text{Eq. S-5}$$

$$\frac{\partial f}{\partial \delta_{w\,LS}} = -(\delta_{HS} - \delta_{LS}) \cdot \frac{\delta_{sample} - \delta_{w\,LS}}{(\delta_{W\,HS} - \delta_{w\,LS})^2} \quad \text{Eq. S-6}$$

$$\frac{\partial f}{\partial \delta_{w\,sample}} = (\delta_{HS} - \delta_{LS}) \cdot \frac{\delta_{HS} - \delta_{LS}}{\delta_{w\,HS} - \delta_{w\,LS}} \quad \text{Eq. S-7}$$

The uncertainty for the $\Delta'^{17}O$ measurement of each sample replicate was determined by taking the standard error of the mean (SEM) from the last three injections. After calculating the uncertainties for each parameter, the error-weighted mean of each replicate measurement (x) was derived, along with their combined uncertainty (u). The following were the equations used:

$$x_{weighted\ average} = \frac{\sum w_i x_i}{\sum w_i} \quad \text{Eq. S-8}$$

$$u_{weighted\ average} = \frac{1}{\sqrt{\sum w_i}} \quad \text{Eq. S-9}$$

where the subscript *'i'* represent the replicates, and *w* as the weight of each replicate, calculated using:

$$w_i = \frac{1}{{u_i}^2} \quad \text{Eq. S-10}$$

The final reported uncertainty for $\Delta'^{17}O$ also accounts for the number of successful injections ($6 \leq n \leq 9$) to adjust for small-sample uncertainty. This was accomplished by multiplying the derived standard error of the mean by the appropriate Student's t-factor at 1σ for the corresponding degrees of freedom (BIPM *et al.*, 2008; Pierchala *et al.*, 2021).

Monte Carlo Implementation of the Lake Isotopic Mass Balance Equation

1. Parametrization

This section details how parameters and input distributions for the Monte Carlo calculations were set up to estimate the output values for humidity and X_e and their associated uncertainties.

1.1. Equilibrium and kinetic fractionation factors

The equilibrium fractionation factors (α_{eq}) for $\delta^{18}O$ and $\delta^{2}H$ are determined through empirical equations as functions of temperature (T), in Kelvin. In this work, we adopt the equations derived by Horita and Wesolowski (1994) using the convention where $\alpha_{eq} > 1$, representing the isotopic ratio in the liquid over the vapor:

$$10^3 ln\ \alpha_{eq}\ (^{18}O) = -7.685 + 6.7123\left(\frac{10^3}{T}\right) - 1.6664\left(\frac{10^6}{T^2}\right) + 0.35041\left(\frac{10^9}{T^3}\right) \quad \text{Eq. S-11}$$

$$10^3 ln\ \alpha_{eq}\ (^{2}H) = 1158.8\left(\frac{T^3}{10^9}\right) - 1620.1\left(\frac{T^2}{10^6}\right) + 794.84\left(\frac{T}{10^3}\right) - 161.04 + 2.9992\left(\frac{10^9}{T^3}\right) \quad \text{Eq. S-12}$$

We derive the equilibrium fractionation factor for $\delta^{17}O$ through its relationship with $\delta^{18}O$, using a θ value of 0.529 applied for equilibrium fractionation (Barkan and Luz, 2007):

$$^{17}\alpha_{eq} = \left(^{18}\alpha_{eq}\right)^{\theta} \quad \text{Eq. S-13}$$

Additionally, we adopt the following kinetic fractionation factors representing pure molecular diffusion (α_{diff}) of $\delta^{18}O$ and $\delta^{2}H$ experimentally derived by Merlivat (1978), and of $\delta^{17}O$ as calculated by Barkan and Luz (2007): α_{diff} ($\delta^{18}O$) = 1.0285, α_{diff} ($\delta^{2}H$) = 1.0251, and α_{diff} ($\delta^{17}O$) = 1.0146. Notably, α_{diff} ($\delta^{17}O$) can also be calculated theoretically from α_{diff} ($\delta^{18}O$) using Eq. S-13 and by applying a θ of 0.5185 (Barkan and Luz, 2007), yielding 1.0147, which closely resembles the experimentally derived value.

To account for turbulence in natural settings, an exponent of n = 0.5 is applied to the α_{diff} values (Horita, *et al.*, 2008), which accounts for the magnitude of kinetic fractionation occurring above open water bodies consistent with most lake studies (Gonfiantini, 1986; Gibson *et al.*, 2016a). The following are the values used as inputs to the calculations: α_{diff} ($\delta^{18}O$) = 1.0141, α_{diff} ($\delta^{2}H$) = 1.0125, and α_{diff} ($\delta^{17}O$) = 1.0073. Fig. S-3 shows the response of the modelled lake isotopic composition to varying *n* values.

1.2. Isotopic composition of atmospheric moisture (δ_A)

The isotopic composition of the atmospheric moisture is estimated by assuming an equilibrium isotopic exchange between precipitation and atmospheric moisture, as described by the following equation (Gibson *et al.*, 2016a):

$$\delta_A = \frac{\left(\delta_p - k\varepsilon^+\right)}{\left(1 + 10^{-3} \cdot k\varepsilon^+\right)} \quad \text{Eq. S-14}$$

where δ_P is the evaporation-flux weighted annual mean isotopic composition of precipitation, k is the seasonality factor, and ε^+ is equilibrium enrichment factor, defined as $1000(\alpha_{eq} - 1)$. The δ_P used in this study was derived from precipitation samples collected from Utah State University (USU) and Utah Valley University (UVU) campuses, with evaporation rate data extracted from the North American Regional Reanalysis (NARR, Mesinger *et al.*, 2006) dataset. Because monthly evaporation rates were explicitly accounted for, the influence of seasonality is inherently incorporated; hence we set the seasonality factor k to 1. Typical k values for temperate climates are ~0.75 to correct for seasonality when mean annual precipitation isotopic composition is used (Gibson *et al.*, 2016a, 2016b). Custado *et al.* (2025) quantified a 76% separation between δ_A derived from the mean annual δ_P, which estimates equilibrium enrichment (ε^+) and δ_A derived from the δ_P that accounts for evaporation rates, which is the effective equilibrium enrichment ($\varepsilon_{effective}$; Gibson *et al.*, 2016a).

1.3. Probability distributions of input parameters

Inflow (δ_I) and lake (δ_S) isotopic composition

We adopt a pure Monte Carlo method for generating input distributions for the inflow and lake isotopic composition to capture the spread within the measured samples for each input parameter (Davis *et al.*, 2015). Specifically for this work, we constructed our input distributions based on Gaussian mixture modelling (GMM) concepts (Terejanu *et al.*, 2008; McLachlan *et al.*, 2019), transforming each data point into normal distributions centred on the observed value with its variance defined by their corresponding analytical uncertainty. The final input distributions are effectively empirical Gaussian mixtures, as they are generated by equally sampling from the measurement-based normal distributions through Monte Carlo methods. This method explicitly propagates analytical uncertainty and limits assumptions on the underlying distribution for each isotopic parameter, considering the temporal and sample size limitations of our dataset. This is particularly important for $\Delta'^{17}O$ whose reported analytical uncertainties can reach up to 15 to 20 per meg.

The input distribution for the inflow isotopic composition is generated by constructing separate distributions for each inflow component: inlet (n = 1), creeks (n = 18), groundwater (n = 6), and precipitation (n = 19). The components are then averaged by using the volumetric contribution of each component to the lake as the weighing factor. For the lake isotopic composition, input distribution is generated from data from 7 measured samples.

Evaporation flux-weighted isotopic composition of precipitation (δ_P)

Input distributions for evaporation flux-weighted precipitation were constructed to explicitly preserve covariance of $\delta^{18}O$ to $\delta^{17}O$ and $\delta^{2}H$ following the Global Meteoric Water Line (GMWL). This reflects the assumption that precipitation is largely influenced by mass-dependent equilibrium fractionation processes during condensation and Rayleigh distillation, which strongly influence individual isotopes but limits variability in the slope, particularly relative to the deviation observed in surface waters (Dansgaard, 1964; Luz and Barkan, 2010; Aron *et al.*, 2021).

First, normal distributions of $\Delta'^{17}O$ and d-excess were generated from the mean and combined uncertainties of the measured precipitation samples. These distributions were then used to generate $\delta^{17}O$ and $\delta^{2}H$ values from $\delta^{18}O$ values via Equations 4 and 5 in the main text, explicitly preserving the GMWL relationship (Eqs. 4 and 5 in the main text). Additional noise from the spread of the measured $\delta^{17}O$ and $\delta^{2}H$ values and their corresponding analytical uncertainties were incorporated into the distributions.

Probability distribution for evaporation flux-weighted temperature

A normal distribution for temperature centred on the evaporation flux-weighted temperature was generated whose spread is based on the weighted variance of the monthly temperature data extracted from the NARR dataset. We chose normal distributions for most of the parameters as a reasonable first-order approximation of the variability in the available datasets.

2. Model implementation

For each isotopic system, relative humidity and X_e are calculated simultaneously by applying the mass balance equation (Eq. 1 in the main text) to each isotope, forming a system of two nonlinear equations for both $\delta^{18}O$-$\delta^{2}H$ (one equation each for $\delta^{18}O$ and $\delta^{2}H$) and triple oxygen (one equation each for $\delta^{17}O$ and $\delta^{18}O$). The constructed systems of equations are then solved using the Python scientific computing library (SciPy; Virtanen *et al.*, 2020). Specifically, the calculations were implemented using the *fsolve* function within SciPy's *optimize* package, which employs a modified Powell's hybrid method. This optimization algorithm iteratively solves systems of nonlinear equations by combining Gauss-Newton methods with gradient descent, allowing for rapid convergence and numerical stability (Powell, 1970).

Monte Carlo simulations are implemented by generating distributions of the input parameters with 100, 000 realizations. The lake mass balance calculations are performed for each realization to estimate relative humidity and X_e values and their associated uncertainties. All calculations are executed using Python scripts available through the link provided in the *Datasets and code* section.

3. Sensitivity analysis

The sensitivities of lake isotopic composition, relative humidity, and X_e to variations in isotopic and environmental (temperature and relative humidity) parameters were evaluated using the same Monte Carlo implementation of the lake mass balance calculations. Normal distributions (n = 100,000) of the input parameters were generated based on the median values and interquartile ranges (IQR) calculated from the initial Monte Carlo simulations. Similar to the treatment of evaporation flux-weighted precipitation, the covariance between among the isotopes was preserved assuming that large-scale atmospheric variability is governed primarily by mass-dependent equilibrium fractionation and mixing, following the GMWL. To systematically limit extreme outputs while keeping the inputs within plausible values, the generated normal distributions were truncated within one standard deviation, retaining realizations that are within the 15.9th and 84.1st percentiles.

The sensitivity of the lake isotopic composition was evaluated at three X_e values (0, 0.3, and 1) with humidity, temperature, and the isotopic compositions of inflow and atmospheric moisture serving as inputs. Meanwhile, the sensitivity of relative humidity and X_e parameters was evaluated with respect to variations in temperature and the isotopic compositions of inflow, lake, and atmospheric moisture.

Reconstruction of the $\delta^{18}O$ Composition of Unevaporated Catchment Precipitation ($\delta^{18}O_{rucp}$)

The equations for the reconstruction of the isotopic composition of the source are adopted from the work of Passey and Ji (2019) and Katz *et al.* (2023):

$$\lambda_{lake} = A \times \left(\Delta'^{17}O_{lake}\right)^3 + B \times \left(\Delta'^{17}O_{lake}\right)^2 + C \times \Delta'^{17}O_{lake} + D \quad \text{Eq. S-15}$$

$$\delta'^{18}O_{rucp} = \frac{\Delta'^{17}O_{MWL} - \delta'^{17}O_{lake} + (\lambda_{lake} - \lambda_{ref})\delta'^{18}O_{lake}}{\lambda_{lake} - \lambda_{ref}} \quad \text{Eq. S-16}$$

where λ_{lake} represents the slope in $\delta'^{17}O$-$\delta'^{18}O$ space between the source and lake waters. The subscripts lake, MWL (Meteoric Water Line), and rucp (reconstructed unevaporated catchment precipitation) denote the water whose isotopic composition is used in the calculation. We assume that the MWL has a slope of $\lambda_{ref} = 0.528$ and an intercept of $\Delta'^{17}O$ = 32 per meg (Passey and Ji, 2019).

Eq. S-15 is the general form of the polynomial that fit the data from modelled $\Delta'^{17}O$ and λ_{lake} values based on isotopic data from the western United States (Passey and Ji, 2019) and later expanded with other lake datasets (Katz *et al.*, 2023). Table S-5 summarizes the coefficients (A, B, C, D) derived from these modelling exercises.

Supplementary Tables

Table S-1 Volumetric discharge value of each inflow component used in the calculations.

Parameter	Value	Uncertainty*	Calculation	Data source*
Upstream (through inlet canal) (f_U, m^3/yr)	3.18 x 10^8	3 to 6%	Mean	USGS
Creeks (f_C, m^3/yr)	1.45 x 10^8	3 to 6%	Mean	USGS and Utah DEQ
Precipitation (f_P, m^3/yr)	1.08 x 10^8	-	Mean	NARR
Groundwater (f_g, m^3/yr)	7.62 x 10^4	1.6 to 2.3%	-	Custado *et al.* (2025)

**Estimated uncertainty values for United States Geological Survey (USGS) discharge measurements from Sauer and Meyer (1992); estimated groundwater flux uncertainty from Custado et al. (2025).*
*** USGS and Utah Department of Environment Quality (Utah DEQ) retrieved from the National Water Interface System (NWIS) database (USGS, 2024); North American Regional Reanalysis (NARR; Mesinger et al., 2006)*

Table S-2 Distributions of input parameters used for the Monte Carlo calculations.

Parameter	Isotope	Input distribution (Fig. S-1)	Mean	Standard deviation	Median	IQR*		Reference data
Temperature (°C)	-	Normal	11.119	8.147	11.124	5.640 – 16.624		Evaporation flux weighted; NWS** data
α_{eq}	$\delta^{18}O$	Normal	1.011	0.001	1.011	1.010 – 1.011		Calculated from temperature (Eq. S-11)
	$\delta^{17}O$	Normal	1.006	0.0004	1.006	1.005 – 1.006		Calculated from α_{eq} ($\delta^{18}O$) (θ = 0.529, Eq. S-13)
	$\delta^{2}H$	Normal	1.096	0.011	1.095	1.088 – 1.103		Calculated from temperature (Eq. S-12)
α_{diff}	$\delta^{18}O$	n.a.	1.014	n.a.	n.a.	n.a.		Kinetic fractionation at zero humidity; 1.0285^{n}, where n = 0.5 (Merlivat, 1978; Voigt *et al.*, 2021)
	$\delta^{17}O$	n.a.	1.007	n.a.	n.a.	n.a.		Kinetic fractionation at zero humidity; 1.0146^{n}, where n = 0.5 (Merlivat, 1978; Voigt *et al.*, 2021)
	$\delta^{2}H$	n.a.	1.012	n.a.	n.a.	n.a.		Kinetic fractionation at zero humidity; 1.0251^{n}, where n = 0.5 (Merlivat, 1978; Voigt *et al.*, 2021)
Total inflow	$\delta^{18}O$ (‰)	Non-normal	-15.479	0.848	-15.603	-16.167 – -14.927		Measured inlet, creeks, amount-weighed precipitation, groundwater, and spring samples
	$\Delta'^{17}O$ (per meg)	Normal (slightly skewed)	19.636	7.630	19.250	14.302 – 24.719		
	$\delta^{2}H$ (‰)	Non-normal	-116.471	6.445	-117.481	-121.496 – -112.074		

**Interquartile Range, range between the 25th and 75th percentile in the distribution*
***National Weather Station (https://www.ncdc.noaa.gov/cdo-web/), Lifton pump station in Idaho (42.123, -111.3133)*

Table S-2 continued.

Parameter	Isotope	Input distribution (Fig. S-1)	Mean	Standard deviation	Median	IQR*		Reference data
Precipitation	$\delta^{18}O$ (‰)	Normal	-11.122	3.340	-11.120	-13.371 – -8.860		Evaporation flux-weighted; Measured precipitation samples
	$\Delta'^{17}O$ (per meg)	Normal	35.064	22.017	35.058	20.142 – 49.914		
	$\delta^{2}H$ (‰)	Normal	-82.808	36.846	-82.743	-107.686 – -57.910		
Atmospheric moisture	$\delta^{18}O$ (‰)	Normal	-21.548	3.382	-21.546	-23.849 – -19.259		Calculated from evaporation flux-weighted precipitation (Eq. S-14)
	$\Delta'^{17}O$ (per meg)	Normal	35.064	22.017	35.058	9.556 – 39.314		
	$\delta^{2}H$ (‰)	Normal	-163.209	10.910	-162.977	-186.545 – -139.720		
Lake	$\delta^{18}O$ (‰)	Non-normal	-9.098	0.101	-9.095	-9.189 – -8.999		Measured lake samples
	$\Delta'^{17}O$ (per meg)	Normal	-2.892	9.878	-2.525	-8.732 – 3.582		
	$\delta^{2}H$ (‰)	Near normal	-84.789	0.492	-84.768	-85.185 – -84.403		

**Interquartile Range, range between the 25th and 75th percentile in the distribution*
***National Weather Station (https://www.ncdc.noaa.gov/cdo-web/), Lifton pump station in Idaho (42.123, -111.3133)*

Table S-3 Summary statistics of output distributions

Parameter	Isotope system	Output distribution (Fig. S-2)	Mean	Standard deviation	Median	IQR*
Relative humidity	Triple oxygen	Non-normal	0.561	0.251	0.590	0.375 – 0.774
	$\delta^{18}O$-$\delta^{2}H$	Non-normal	0.607	0.235	0.639	0.455 – 0.788
Evaporation/ Inflow (X_e)	Triple oxygen	Skewed normal	0.292	0.114	0.267	0.231 – 0.308
	$\delta^{18}O$-$\delta^{2}H$	Skewed normal	0.294	0.112	0.281	0.240 – 0.321

**Interquartile Range, range between the 25th and 75th percentile in the distribution*

Table S-4 Monthly climatological means of climate data used.

Month	Relative humidity, %	Evaporation, kg/m^2	Precipitation rate, kg/m^2/s	Temperature, °F
Jan	-	0.050	1.12E-05	18.4
Feb	-	0.069	1.30E-05	19.4
Mar	-	0.118	1.09E-05	28.6
Apr	63.91	0.204	1.44E-05	39.1
May	64.18	0.340	1.64E-05	49.3
Jun	62.39	0.455	1.20E-05	59.3
Jul	53.70	0.409	8.31E-06	68
Aug	59.00	0.274	8.77E-06	65
Sep	56.48	0.155	1.26E-05	55.8
Oct	61.99	0.084	1.35E-05	43.7
Nov	72.48	0.068	1.27E-05	31.2
Dec	-	0.049	1.23E-05	21

**Relative humidity data were extracted from USGS Station 415941111175401 (41.99471667, −111.2984667) and span May 2022 to November 2024; no data were reported for January, February, March, and December. The evaporation flux-weighted relative humidity cited in the main text was calculated assuming that months without data were fully saturated (h = 1), representing an upper-bound limit for these months. Evaporation and precipitation rates were obtained from the North American Regional Reanalysis (NARR) dataset; temperature data were obtained from the Lifton Pumping Station, ID (https://www.ncdc.noaa.gov/cdo-web/; 42.123, −111.315), covering the period 2000–2024. Lake stations marked as stars in Fig. 1b.*

Table S-5 $\delta^{18}O_{rucp}$ reconstructions using different coefficients (A, B, C, D) derived by Katz *et al.* (2023) and Passey and Ji (2019). These coefficients are applied to Eq. S-15.

λ_{lake}*	$\delta^{18}O_{rucp}$ (‰)*	A	B	C	D	Humidity range	Equation used
0.5228	-15.670 (IQR: -16.155 – -15.241)	9.8941	1.2759	0.0580	0.5229	Full (0.3 to 0.9)	Katz *et al.* (2023)
0.5235	-16.842 (IQR: -17.539 – -16.243)	1.9600	0.5340	0.0599	0.5237	Low (0.3 to 0.7)	Katz *et al.* (2023)
0.5213	-14.265 (IQR: -14.629 – -13.942)	40.9869	1.9363	0.0701	0.5215	High (0.7 to 0.9)	Katz *et al.* (2023)
0.5234	-16.672 (IQR: -17.340 – -16.095)	1.9856	0.5730	0.0601	0.5236	Western US (0.3 to 0.7)	Passey and Ji (2019)
0.5246	-18.066 (IQR: -21.261 – -15.851)	-	-	-	-	-	Inflow and lake data

**Median and IQR values are from 100,000 Monte Carlo simulations. The IQRs for the calculated λ_{lake} values are 0.0026 (Inflow and lake data) and 0.0007 (Passey and Ji, 2019, Katz et al., 2023).*

Table S-6 External standards used for the calibration of internal reference standards (VSMOW2, USGS53, USGS47) and data quality check (USGS46).

Standard	$\delta^{17}O$ (‰)	$\delta^{17}O$ uncertainty	$\delta^{18}O$ (‰)	$\delta^{18}O$ uncertainty	$\delta^{2}H$ (‰)	$\delta^{2}H$ uncertainty	Reference
VSMOW2	0	0.03	0	0.02	0	0.4	IAEA, 2017
USGS53	2.85	0.01	5.47	0.03	40.2	0.4	USGS, 2018; Berman *et al.*, 2013
USGS46	-15.85	0.02	-29.8	0.03	-235.9	0.7	USGS, 2019a, Berman *et al.*, 2013
USGS47	-10.47	0.02	-19.8	0.02	-150.2	0.5	USGS, 2019b; Hutchings and Konecky, 2023

Table S-7 Internal standards used for data normalization and drift correction. The $\Delta'^{17}O$ of each replicate was calculated from the $\Delta'^{17}O$ value of each of the last three injections.

Standard	Date	$\delta^{17}O$ (‰)	$\delta^{17}O$ (1σ, ‰,)	$\delta^{18}O$ (‰)	$\delta^{18}O$ (1σ, ‰,)	$\delta^{2}H$ (‰)	$\delta^{2}H$ (1σ, ‰,)	$\Delta'^{17}O$ (per meg)	$\Delta'^{17}O$ (SEM, per meg)	*n* replicates
Heavy	6/7/2024	2.640	0.028	5.039	0.024	2.967	0.193	-19.351	10.858	2
Light	6/7/2024	-8.711	0.027	-16.395	0.022	-97.684	0.327	-26.343	11.397	2
Drift	6/7/2024	-2.000	0.015	-3.794	0.015	-16.451	0.133	-16.811	3.355	6
USGS46	6/7/2024	-15.689	0.056	-29.491	0.048	-228.800	0.813	-5.984	20.100	2
Heavy	6/9/2024	2.625	0.031	5.016	0.023	2.967	0.185	-22.855	10.099	2
Light	6/9/2024	-8.706	0.033	-16.392	0.020	-97.679	0.313	5.416	9.869	2
Drift	6/9/2024	-2.014	0.015	-3.786	0.013	-16.516	0.111	-4.066	7.602	6
USGS46	6/9/2024	-15.578	0.046	-29.315	0.031	-227.517	0.785	4.888	15.677	2
Heavy	6/11/2024	2.622	0.036	5.020	0.046	2.929	0.220	-32.852	7.553	2
Light	6/11/2024	-8.727	0.046	-16.417	0.052	-97.673	0.379	-27.389	10.186	2
Drift	6/11/2024	-1.984	0.016	-3.791	0.021	-16.634	0.129	-3.500	2.174	6
USGS46	6/11/2024	-15.776	0.060	-29.576	0.073	-228.458	0.859	-39.039	5.770	2
Heavy	6/14/2024	2.621	0.018	5.000	0.016	2.953	0.176	-40.110	18.083	2
Light	6/14/2024	-8.700	0.025	-16.350	0.031	-97.518	0.320	-38.770	4.999	2
Drift	6/14/2024	-2.022	0.020	-3.809	0.015	-16.218	0.155	-6.708	6.802	6
USGS46	6/14/2024	-15.683	0.039	-29.512	0.057	-228.298	0.803	47.843	25.414	2
Heavy	6/17/2024	2.626	0.036	5.020	0.029	2.963	0.289	-22.050	16.298	2
Light	6/17/2024	-8.748	0.018	-16.417	0.016	-97.800	0.328	3.567	15.616	2
Drift	6/17/2024	-1.992	0.019	-3.803	0.014	-16.658	0.161	6.526	5.402	6
USGS46	6/17/2024	-15.590	0.034	-29.352	0.033	-226.589	0.760	14.081	8.120	2
Heavy	6/20/2024	2.631	0.058	5.071	0.085	3.036	0.399	-21.232	15.567	2
Light	6/20/2024	-8.716	0.034	-16.395	0.019	-97.680	0.339	-24.346	14.607	2
Drift	6/20/2024	-1.970	0.022	-3.728	0.026	-16.224	0.190	18.910	8.695	6
USGS46	6/20/2024	-15.702	0.043	-29.564	0.042	-229.235	0.716	17.417	5.846	2

Supplementary Figures

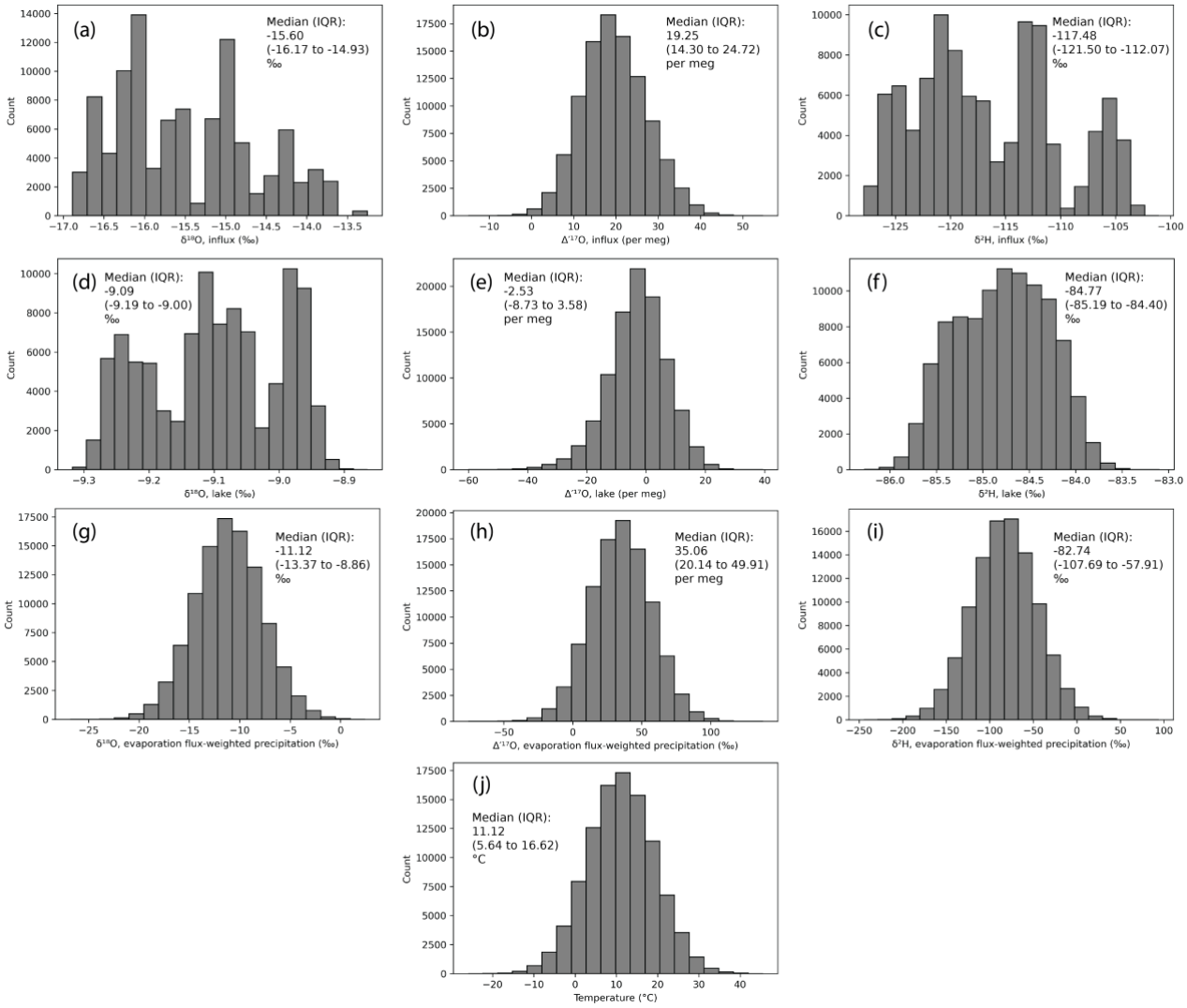

Figure S-1 Histograms of the generated input distributions as described in the Parametrization section (n = 100,000). From top left, proceeding horizontally: **(a)** $\delta^{18}O$ of influx, **(b)** $\Delta'^{17}O$ of influx, **(c)** $\delta^{2}H$ of influx, **(d)** $\delta^{18}O$ of lake, **(e)** $\Delta'^{17}O$ of lake, **(f)** $\delta^{2}H$ of lake, **(g)** $\delta^{18}O$ of evaporation flux-weighted precipitation, **(h)** $\Delta'^{17}O$ of evaporation flux-weighted precipitation, **(i)** $\delta^{2}H$ of evaporation flux-weighted precipitation, and **(j)** temperature.

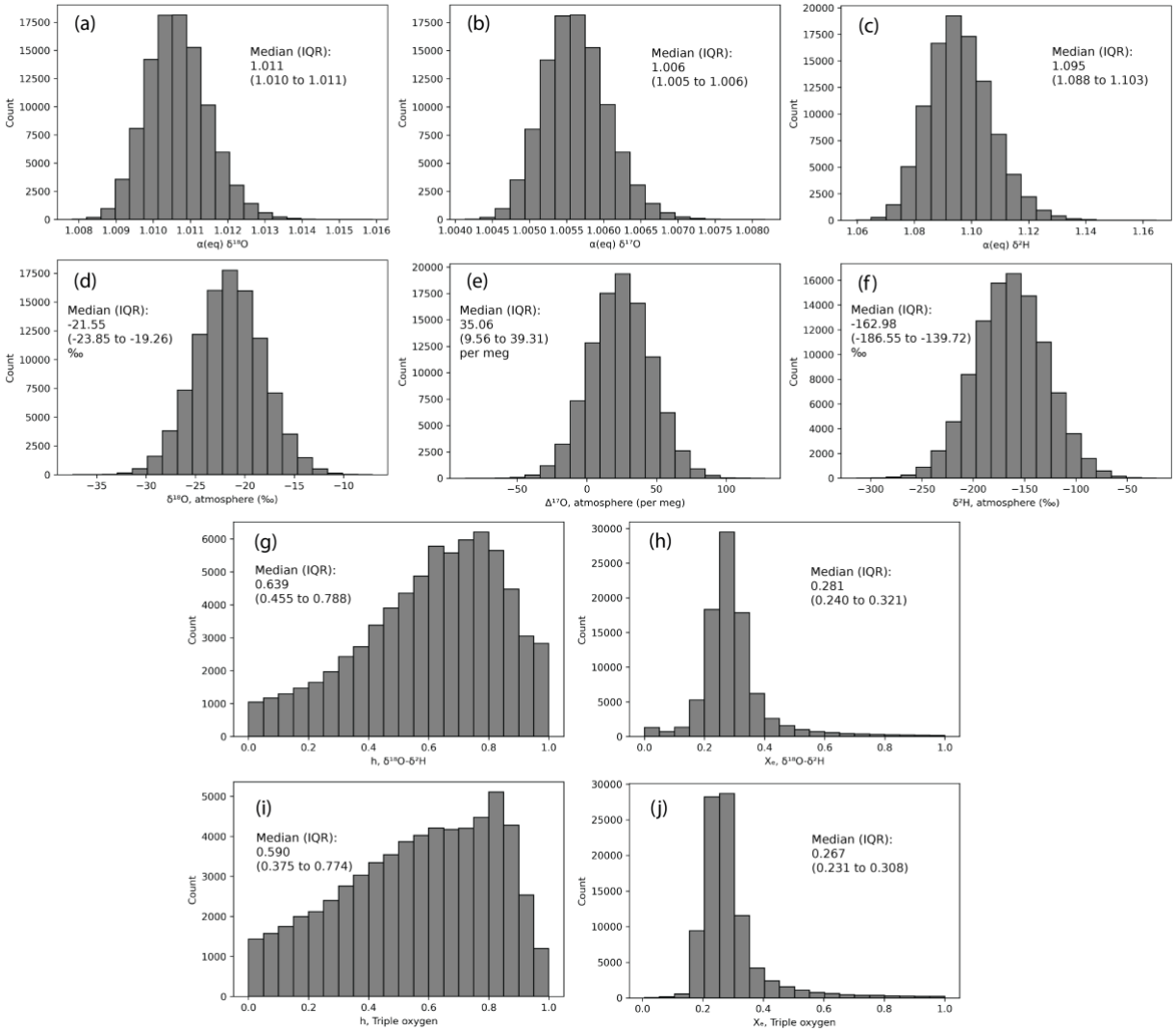

Figure S-2 Histograms of the calculated output distributions from Monte Carlo simulations of the isotopic lake mass balance (n = 100,000). From top left, proceeding horizontally: Equilibrium fractionation factors (α_{eq}) calculated from the range of input temperatures for **(a)** $\delta^{18}O$, **(b)** $\delta^{17}O$, and **(c)** $\delta^{2}H$; **(d)** atmospheric moisture isotopic compositions for **(d)** $\delta^{18}O$, **(e)** $\Delta'^{17}O$, and **(f)** $\delta^{2}H$; calculated **(g)** humidity and **(h)** X_e in the $\delta^{18}O$- $\delta^{2}H$ space; calculated **(i)** humidity and **(j)** X_e in the triple oxygen space.

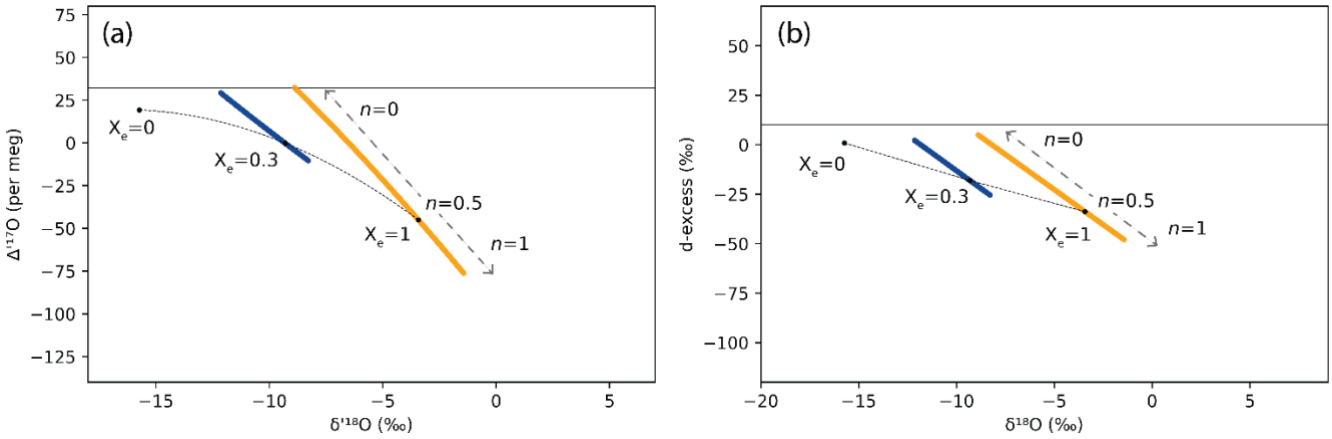

Figure S-3 Sensitivity plots of the lake isotopic composition to the turbulence parameter (n) in the **(a)** triple oxygen ($\delta'^{18}O$ vs. $\Delta'^{17}O$) and **(b)** $\delta^{18}O$-$\delta^{2}H$ ($\delta^{18}O$ vs. d-excess) spaces at increasing X_e. The value of n was varied from 0 (turbulent diffusion endmember; $\alpha_{diff} = 1$) to 1 (molecular diffusion endmember; $\alpha_{diff} = 1.0285$ for $\delta^{18}O$, 1.0251 for $\delta^{2}H$, and 1.0146 for $\delta^{17}O$; Merlivat, 1978; Barkan and Luz, 2007). Gray dashed lines indicate the direction of change in lake isotopic composition. Because direct constraints on n were not available for Bear Lake, we adopted the commonly used value of n = 0.5 and focused the Monte Carlo analysis of the isotopic parameters. As n approaches 1, corresponding to increasingly molecular diffusion-dominated transport, lake waters become isotopically heavier in $\delta^{18}O$ and lighter in $\Delta'^{17}O$ and d-excess, reflecting enhanced kinetic fractionation. Conversely, as n approaches 0, the term $\alpha_{eq}\alpha_{diff}$ in Eq. 1 approaches α_{eq}, indicating the breakdown of the laminar boundary layer described in the Craig–Gordon model and the increasing dominance of turbulent transport.

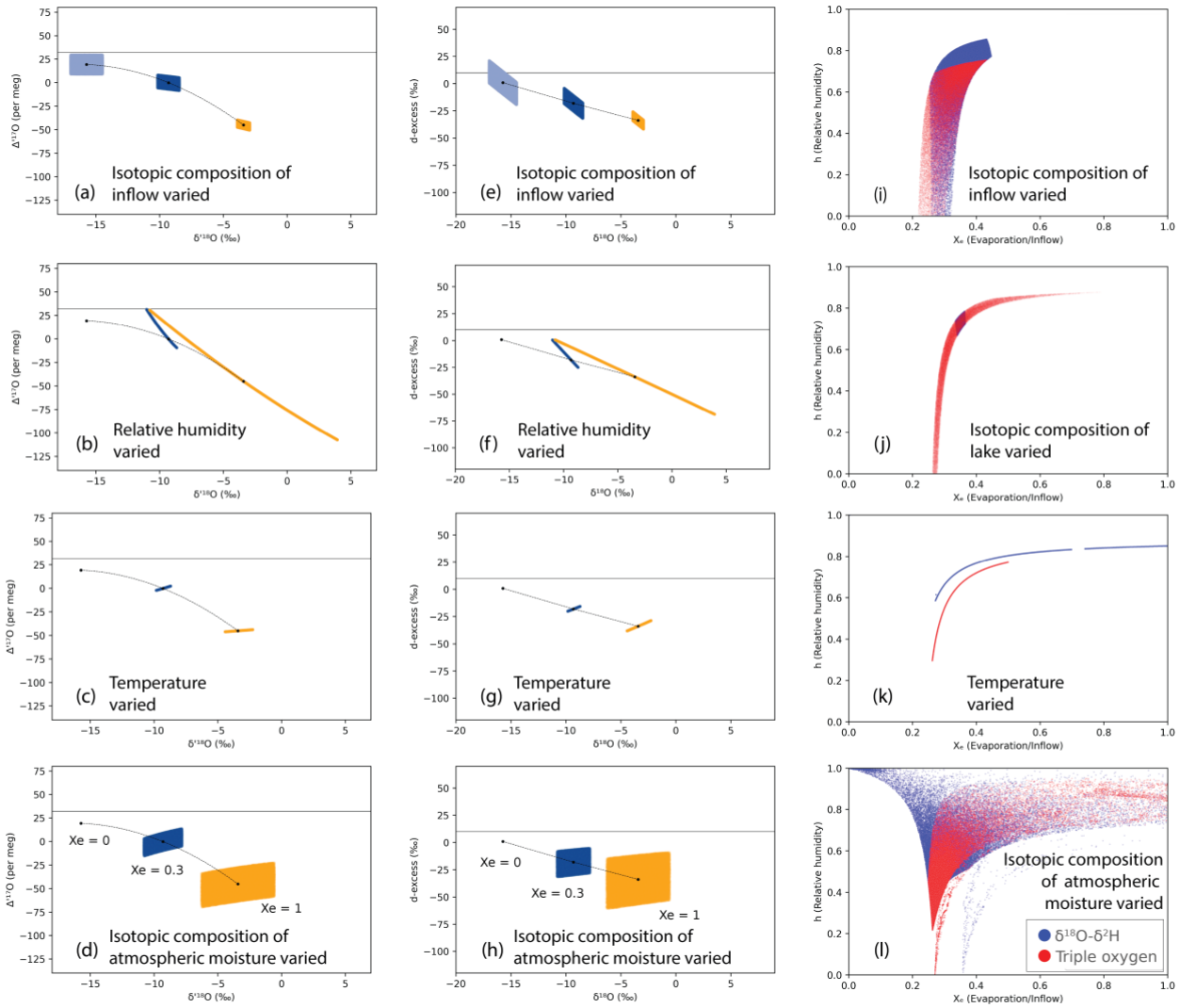

Figure S-4 Sensitivity plots of the lake isotopic composition in the triple oxygen ($\delta'^{18}O$ vs. $\Delta'^{17}O$, left column) and $\delta^{18}O$-$\delta^{2}H$ ($\delta^{18}O$ vs. d-excess, middle column) spaces, and sensitivity of relative humidity and X_e in both isotopic systems (X_e vs. h, right column). The lake isotopic composition is simulated for X_e values of 0, 0.3, and 1; lines represent evaporation trajectory based on the available isotopic data. The left and middle columns illustrate changes in lake isotopic composition as individual input parameters are varied (with all others held constant): **(a, e)** inflow isotopic composition, **(b, f)** relative humidity, **(c, g)** temperature, and **(d, h)** atmospheric moisture isotopic composition. Right column shows changes in relative humidity and X_e with the following parameters held constant: **(i)** inflow isotopic composition, **(j)** lake isotopic composition, **(k)** temperature, and **(l)** atmospheric moisture isotopic composition. All plots are derived from Monte Carlo mass balance simulations (n = 100,000) using normally distributed input parameters.

Supplementary Information References

Aron, P.G., Levin, N.E., Beverly, E.J., Huth, T.E., Passey, B.H., Pelletier, E.M., Poulsen, C.J., Winkelstern, I.Z., Yarian, D.A. (2021) Triple oxygen isotopes in the water cycle. *Chemical Geology* 565, 120026. https://doi.org/10.1016/j.chemgeo.2020.120026

Barkan, E., Luz, B. (2007) Diffusivity fractionations of $H_2{}^{16}O/H_2{}^{17}O$ and $H_2{}^{16}O/H_2{}^{18}O$ in air and their implications for isotope hydrology. *Rapid Communications in Mass Spectrometry* 21, 2999–3005. https://doi.org/10.1002/rcm.3180

Berman, E.S.F., Levin, N.E., Landais, A., Li, S., Owano, T. (2013) Measurement of $\delta^{18}O$, $\delta^{17}O$, and ^{17}O-excess in Water by Off-Axis Integrated Cavity Output Spectroscopy and Isotope Ratio Mass Spectrometry. *Analytical Chemistry* 85, 10392–10398. https://doi.org/10.1021/ac402366t

BIPM, IEC, IFCC, ILAC, ISO, IUPAC, IUPAP, OIML (2008) *Evaluation of measurement data — Guide to the expression of uncertainty in measurement*. First Edition, Joint Committee for Guides in Metrology.

Birdsey, P. (1989) *The Limnology of Bear Lake, Utah-Idaho, 1912-1988: A Literature Review*. Utah Department of Natural Resources, Publication 89-5, Salt Lake City.

Custado, M.J., Gagnon, C.A., Belanger, B., Sekhon, N., Bernstein-Schalet, J., Kinsley, C.W., Sharp, W.D., Oster, J.L., Ibarra, D.E. (2025) Constraining the Modern Hydrological Balance of Bear Lake, Utah-Idaho: Insights From Stable Isotopes ($\delta^{18}O$ and $\delta^{2}H$). *Water Resources Research* 61, e2024WR038264. https://doi.org/10.1029/2024WR038264

Dansgaard, W. (1964) Stable isotopes in precipitation. *Tellus* 16, 436–468. https://doi.org/10.1111/j.2153-3490.1964.tb00181.x

Davis, P., Syme, J., Heikoop, J., Fessenden-Rahn, J., Perkins, G., Newman, B., Chrystal, A.E., Hagerty, S.B. (2015) Quantifying uncertainty in stable isotope mixing models. *Journal of Geophysical Research: Biogeosciences* 120, 903–923. https://doi.org/10.1002/2014JG002839

Dean, W.E., Forester, R.M., Bright, J., Anderson, R.Y. (2007) Influence of the diversion of Bear River into Bear Lake (Utah and Idaho) on the environment of deposition of carbonate minerals. *Limnology and Oceanography* 52, 1094–1111. https://doi.org/10.4319/lo.2007.52.3.1094

Dean, W.E., Wurtsbaugh, W.A., Lamarra, V.A. (2009) Climatic and limnologic setting of Bear Lake, Utah and Idaho. In: Rosenbaum, J.G., Kaufman, D.S. (Eds.) *Paleoenvironments of Bear Lake, Utah and Idaho, and its catchment*. Geological Society of America, Boulder, Special Paper 450, 1–14. https://doi.org/10.1130/2009.2450(01)

Gibson, J.J., Birks, S.J., Yi, Y. (2016a) Stable isotope mass balance of lakes: a contemporary perspective. *Quaternary Science Reviews* 131, 316–328. https://doi.org/10.1016/j.quascirev.2015.04.013

Gibson, J.J., Birks, S.J., Yi, Y., Moncur, M.C., McEachern, P.M. (2016b) Stable isotope mass balance of fifty lakes in central Alberta: Assessing the role of water balance parameters in determining trophic status and lake level. *Journal of Hydrology: Regional Studies* 6, 13–25. https://doi.org/10.1016/j.ejrh.2016.01.034

Gonfiantini, R. (1986) Environmental Isotopes in Lake Studies. In: Fritz, P., Fontes, J.Ch. (Eds.) *Handbook of Environmental Isotope Geochemistry: Volume 2, The Terrestrial Environment, B*. Elsevier, Amsterdam, 113–168. https://doi.org/10.1016/B978-0-444-42225-5.50008-5

Gröning, M. (2011) Improved water $\delta^{2}H$ and $\delta^{18}O$ calibration and calculation of measurement uncertainty using a simple software tool. *Rapid Communications in Mass Spectrometry* 25, 2711–2720. https://doi.org/10.1002/rcm.5074

Horita, J., Wesolowski, D.J. (1994) Liquid-vapor fractionation of oxygen and hydrogen isotopes of water from the freezing to the critical temperature. *Geochimica et Cosmochimica Acta* 58, 3425–3437. https://doi.org/10.1016/0016-7037(94)90096-5

Horita, J., Rozanski, K., Cohen, S. (2008) Isotope effects in the evaporation of water: a status report of the Craig–Gordon model. *Isotopes in Environmental and Health Studies* 44, 23–49. https://doi.org/10.1080/10256010801887174

Hutchings, J.A., Konecky, B.L. (2023) Optimization of a Picarro L2140-i cavity ring-down spectrometer for routine measurement of triple oxygen isotope ratios in meteoric waters. *Atmospheric Measurement Techniques* 16, 1663–1682. https://doi.org/10.5194/amt-16-1663-2023

IAEA (2017) *Reference Sheet for International Meaurement Standards*. International Atomic Energy Agency, Vienna.

Kaliser, B.N. (1972) *Environmental Geology of Bear Lake Area, Rich County, Utah*. Utah Geological and Mineralogical Survey, Bulletin 096, Salt Lake City.

Katz, S.A., Levin, N.E., Rodbell, D.T., Gillikin, D.P., Aron, P.G., Passey, B.H., Tapia, P.M., Serrepe, A.R., Abbott, M.B. (2023) Detecting hydrologic distinctions among Andean lakes using clumped and triple oxygen isotopes. *Earth and Planetary Science Letters* 602, 117927. https://doi.org/10.1016/j.epsl.2022.117927

Luz, B., Barkan, E. (2010) Variations of $^{17}O/^{16}O$ and $^{18}O/^{16}O$ in meteoric waters. *Geochimica et Cosmochimica Acta* 74, 6276–6286. https://doi.org/10.1016/j.gca.2010.08.016

McLachlan, G.J., Lee, S.X., Rathnayake, S.I. (2019) Finite Mixture Models. *Annual Review of Statistics and Its Application* 6, 355–378. https://doi.org/10.1146/annurev-statistics-031017-100325

Merlivat, L. (1978) Molecular diffusivities of $H_2{}^{16}O$, $HD^{16}O$, and $H_2{}^{18}O$ in gases. *The Journal of Chemical Physics* 69, 2864–2871. https://doi.org/10.1063/1.436884

Mesinger, F., DiMego, G., Kalnay, E., Mitchell, K., Shafran, P.C., *et al.* (2006) North American Regional Reanalysis. *Bulletin of the American Meteorological Society* 87, 343–360. https://doi.org/10.1175/BAMS-87-3-343

Passey, B.H., Ji, H. (2019) Triple oxygen isotope signatures of evaporation in lake waters and carbonates: A case study from the western United States. *Earth and Planetary Science Letters* 518, 1–12. https://doi.org/10.1016/j.epsl.2019.04.026

Pierchala, A., Rozanski, K., Dulinski, M., Gorczyca, Z., Czub, R. (2021) Triple-isotope calibration of in-house water standards supplemented by determination of ^{17}O content of USGS49-50 reference materials using cavity ring-down laser spectrometry. *Isotopes in Environmental and Health Studies* 57, 254–261. https://doi.org/10.1080/10256016.2021.1875222

Powell, M.J.D. (1970) A Hybrid Method for Nonlinear Equations. In: Rabinowitz, P. (Ed.) *Numerical Methods for Nonlinear Algebraic Equations*. Gordon and Breach Science, London, 87–144.

Sauer, V.B., Meyer, R.W. (1992) *Determination of error in individual discharge measurements*. U.S. Geological Survey, Norcross, GA, Open-File Report 92-144. https://doi.org/10.3133/ofr92144

Terejanu, G., Singla, P., Singh, T., Scott, P.D. (2008) Uncertainty Propagation for Nonlinear Dynamic Systems Using Gaussian Mixture Models. *Journal of Guidance, Control, and Dynamics* 31, 1623–1633. https://doi.org/10.2514/1.36247

USGS (2018) *Report of Stable Isotopic Composition: Reference Material USGS53*. U.S. Geological Survey, Reston.

USGS (2019a) *Report of Stable Isotopic Composition - Reference Material USGS46*. U.S. Geological Survey, Reston.

USGS (2019b) *Report of Stable Isotopic Composition - Reference Material USGS47*. U.S. Geological Survey, Reston.

USGS (2024) USGS Current Water Data for the Nation. Accessed 10 April 2024. https://waterdata.usgs.gov/

Virtanen, P., Gommers, R., Oliphant, T.E., Haberland, M., Reddy, T., *et al.* (2020) SciPy 1.0: fundamental algorithms for scientific computing in Python. *Nature Methods* 17, 261–272. https://doi.org/10.1038/s41592-019-0686-2

Voigt, C., Herwartz, D., Dorador, C., Staubwasser, M. (2021) Triple oxygen isotope systematics of evaporation and mixing processes in a dynamic desert lake system. *Hydrology and Earth System Sciences* 25, 1211–1228. https://doi.org/10.5194/hess-25-1211-2021